

Article

# Colloidal Photonic Crystals Containing Silver Nanoparticles with Tunable Structural Colors

Chun-Feng Lai \* and Yu-Chi Wang

Department of Photonics, Feng Chia University, Seatwen, Taichung 40724, Taiwan; d0252984@gmail.com

\* Correspondence: chunflai@fcu.edu.tw; Tel.: +886-424-517-250

Academic Editors: Qingfeng Yan and Helmut Cölfen

Received: 13 April 2016; Accepted: 17 May 2016; Published: 19 May 2016

**Abstract:** Polystyrene (PS) colloidal photonic crystals (CPhCs) containing silver nanoparticles (AgNPs) present tunable structural colors. PS CPhC color films containing a high concentration of AgNPs were prepared using self-assembly process through gravitational sedimentation method. High-concentration AgNPs were deposited on the bottom of the substrate and acted as black materials to absorb background and scattering light. Brilliant structural colors were enhanced because of the absorption of incoherent scattering light, and color saturation was increased by the distribution AgNPs on the PS CPhC surfaces. The vivid iridescent structural colors of AgNPs/PS hybrid CPhC films were based on Bragg diffraction and backward scattering absorption using AgNPs. The photonic stop band of PS CPhCs and AgNPs/PS hybrid CPhCs were measured by UV–visible reflection spectrometry and calculated based on the Bragg–Snell law. In addition, the tunable structural colors of AgNPs/PS hybrid CPhC films were evaluated using color measurements according to the Commission International d’Eclairage standard colorimetric system. This paper presents a simple and inexpensive method to produce tunable structural colors for numerous applications, such as textile fabrics, bionic colors, catalysis, and paints.

**Keywords:** colloidal photonic crystals; silver; nanoparticles; structural colors

## 1. Introduction

Structural colors with brilliant iridescent character have attracted considerable attention in a variety of applications [1–3]. Iridescent colors produced by interference, diffraction, or the scattering of light are generated by periodic lattice crystals. Colloidal photonic crystals (CPhCs) of periodic crystals are artificially fabricated, which are capable of reflecting light at a specific photonic stop band (PSB) because of the periodic variation of refractive index in the crystal structures [4,5]. Self-assembly of silica, polystyrene (PS), or polymethyl methacrylate (PMMA) nanospheres into a close-packed array is a simple method for fabrication of 3D CPhC structures [6–8]. However, CPhC structures have several problems, including low color visibility and poor crystal quality because of cracks and an opalescent appearance, which limit its structural color for applications. An effective method for solving low color visibility is to mix black materials with high absorption in the visible light region into colloidal systems to enhance color saturation, because black materials can decrease incoherent scattering, thereby enhancing color [9–12]. Recently, carbon black (CB) [13–16], carbon [17,18], carbon-modified colloidal nanospheres [19,20], and metal nanoparticles (NPs) [21–25] of black materials have been used as additives in fabricating CPhCs with enhanced structural colors.

Incorporation of a variety of NPs in CPhCs results in the production of brilliant iridescent colors [13–25] because NPs can absorb and scatter visible light. Gold (Au) NPs and silver (Ag) NPs have been synthesized using the chemical reduction method [26,27] and the facile wet chemical route method [28], respectively. In the present study, CPhCs were incorporated directly with high concentrations of AgNPs by using a simple method. The localized surface plasmon resonance (LSPR)

of AgNPs can affect the structural colors of AgNPs/PS hybrid CPhC films [21,24]. Therefore, a high concentration of AgNPs was employed in this work to avoid the LSPR effect. The high concentration of AgNPs in the CPhC structures results in absorption of all the wavelengths of visible light and reduces scattering light, thereby remarkably enhancing color, particularly iridescent, tunable structural colors that are visible under natural lighting conditions. The main method for randomly distributing AgNPs on PS nanosphere surface involved electrostatic interactions. In addition, the doping of AgNPs into PS nanospheres and sedimentation on the bottom of the substrate can absorb background and scattering light, because Ag ( $\rho_{\text{Ag}} = 10.49 \text{ g} \cdot \text{cm}^{-3}$ ) is denser than PS ( $\rho_{\text{PS}} = 0.96 \text{ g} \cdot \text{cm}^{-3}$ ), which results in vivid structural colors. The reflection wavelength of PS CPhC films with and without the AgNPs were predicted theoretically and compared with experimental results. The structural colors of the AgNPs/PS hybrid CPhC films were not only substantially enhanced but also varied with observation angles throughout the composition. AgNPs/PS hybrid CPhCs with enhanced structural colors were obtained using a simple and inexpensive method. AgNPs are generally used in biomedical applications as an antimicrobial agent [29] and catalyst [30]. Therefore, CPhCs incorporated with AgNPs could provide additional advantages, such as antibacterial activity, for textile fabrics.

## 2. Results

### 2.1. Optical Properties of High-Concentration AgNPs

AgNPs are used in medicinal purposes owing to its antibacterial, antimicrobial, and anti-inflammatory properties [31,32]. In this study, dispersion of high-concentration AgNPs in water could significantly affect the optical properties. Therefore, we initially evaluated the optical characteristics of the AgNP diluted solutions. Figure 1a shows that the 1.0 and 4.5 weight percent (wt %) diluted solutions in a standard quartz cuvette were black-brown in color because light was absorbed across the entire visible spectrum. The field-emission scanning electron microscopy (FESEM) images in Figure 1b and the field emission transmission electron microscopy (FETEM) images in Figure S1a showed the agglomerated AgNPs. Due to the optical properties of AgNPs upon aggregation, the conduction electrons near each NP surface become delocalized and are shared amongst neighboring NPs. When AgNPs aggregate, the extinction spectra of Figure 1d demonstrated the LSPR of AgNPs, which was not observed in this work. In addition, Figure 1c illustrates the transmittance spectra of AgNPs at different concentrations, in which strong absorption was observed in the visible spectrum. The transmittance dropped to around 5% or less, depending on the concentration of AgNPs. Figure 1d shows the extinction spectra depending on the size, shape, and aggregation state of AgNPs, which are almost entirely caused by photon absorption.

### 2.2. Crystal Structures of the Prepared AgNPs/PS Hybrid CPhC Color Films

Samples with different PS nanosphere sizes (diameter  $D_{\text{PS}}$ ) of 170, 215, and 250 nm and AgNP concentrations were prepared (Table 1). In this study, the polydispersity index (PDI) of the PS nanospheres was also measured by the dynamic light scattering (DLS) method performed using a laser particle size analyzer (LPSA); the results are provided in Table 1 and Figure S2. The AgNPs/PS hybrid CPhC color films were fabricated by mixing with AgNPs via the thermally-assisted self-assembly process through gravitational sedimentation method, which enabled PS nanospheres to assemble into a highly crystalline arrangement with face-centered cubic (*fcc*) crystals. A few drops of AgNPs/PS mixture suspensions (100  $\mu\text{L}$ ) were placed on the cover glass substrate and carefully spread to fully cover the glass surface and placed in an oven at a constant temperature of 50  $^{\circ}\text{C}$  for 2 h, as shown in Figure 2. The oven temperature was then raised to 80  $^{\circ}\text{C}$  for 30 min to improve the physical rigidity of the AgNPs/PS hybrid CPhC color films.

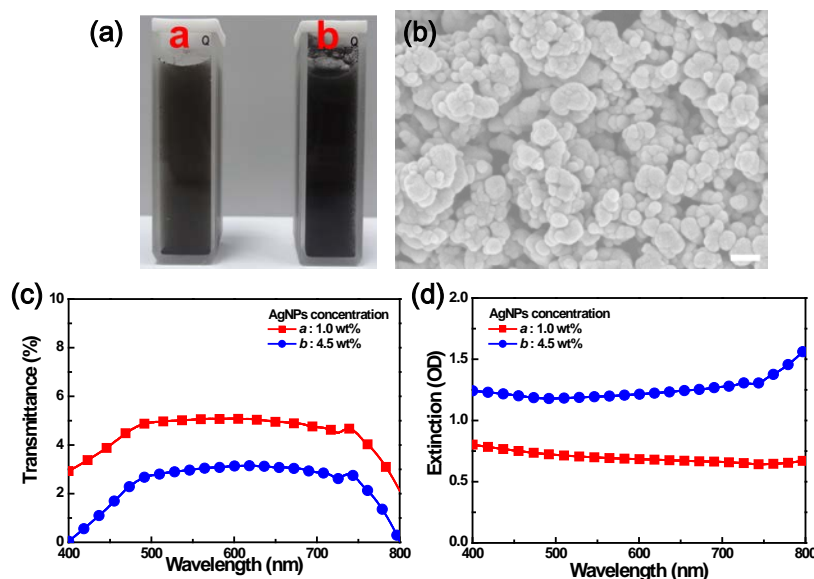


**Figure 1.** (a) Diluted solution appears black-brown because light is absorbed across the entire visible spectrum. (b) Field-emission scanning electron microscopy (FESEM) image of silver nanoparticle (AgNP) agglomerates at 4.5 wt % concentration. Inset scale bar is 200 nm. (c) Transmittance and (d) extinction spectra of AgNPs diluted solutions, which almost entirely to absorb all wavelengths within the visible region with negligible scattering.

**Table 1.** Structural parameters for the three AgNPs/polystyrene (PS) hybrid colloidal photonic crystals (CPhCs) films.

Sample	Diameter ( $D_{PS}$ , nm)		PDI	AgNP Concentrations (wt %)
	FESEM	LPSA		
A	170	189.5	0.040	1.0/4.5
B	215	233.3	0.028	
C	250	267.1	0.043	

FESEM: statistical average diameter measured through FESEM; LPSA: diameter of the PS nanospheres measured by the DLS method.

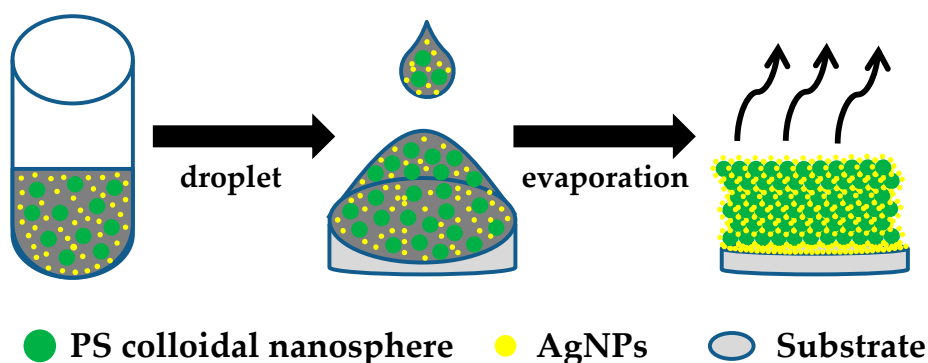


**Figure 2.** Schematic of the thermally assisted self-assembly process through gravitational sedimentation method.

FESEM was used to study the crystalline structure of the AgNPs/PS hybrid CPhC color films. The AgNPs/PS hybrid CPhC color films with different  $D_{PS}$  were grown through the gravitational sedimentation method, with surfaces parallel to the (111) crystallographic plane, as shown in Figure 3a–c. The FESEM images indicated that the AgNP dopant did not disrupt the structures

of CPhCs. The FETEM and energy-dispersive spectrometer (EDS) mapping images of the AgNPs/PS hybrid CPhC films showed that the AgNPs were randomly adsorbed on the PS nanosphere surface (Figure S1b–c and Figure 3d). Figure 3d shows the EDS mapping images of a sample with Ag atom and O atom appeared at the nanospheres. Thus, AgNPs easily adsorbed O atoms, which indicated an antibacterial effect [33,34]. The results suggest that the introduction of AgNPs at high concentrations did not affect the structural quality of the PS CPhC films.

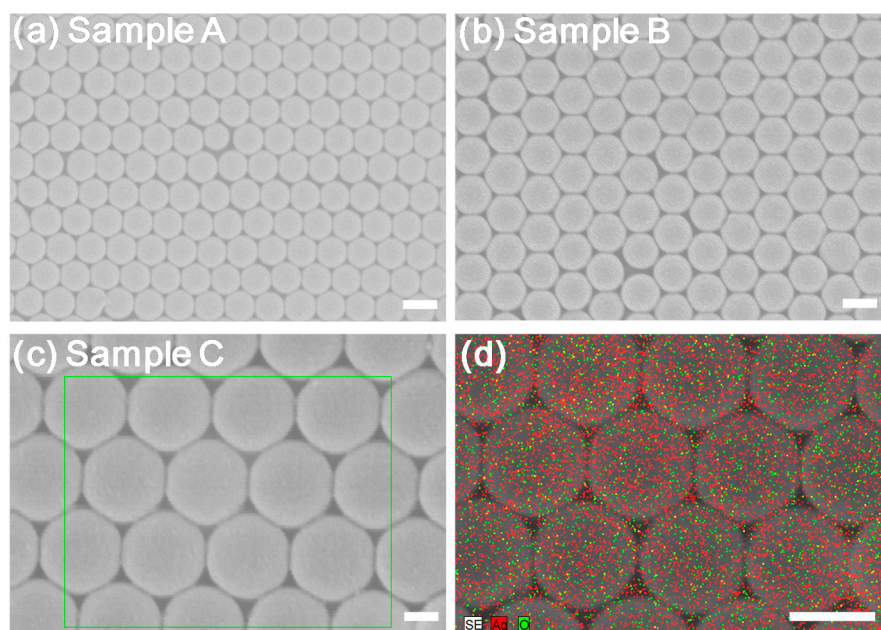


**Figure 3.** FESEM images of PS CPhC structures with 4.5 wt %, AgNPs: (a) sample A; (b) sample B; (c) sample C. (d) EDS compositional mapping (Ag/O overlay) scans from the red dashed line area of image (c). All scale bars are 200 nm.

### 2.3. Effects of AgNPs Content on PS CPhC Color Films

Figure 4 shows the photographs of PS CPhC color films with and without AgNPs. Pure PS CPhC films are usually milky white with extremely faint structural colors (Figure 4b, standard). As shown in Figure 4a, the visual appearance of PS CPhCs markedly changed from a dull color to a vivid iridescent color by introducing AgNPs into PS CPhC structures. The pictures were obtained under normal natural lighting conditions and showed the highly orientation-dependent Bragg diffraction. The pictures indicated a new color mechanism, which should contribute to the absorbance of light scattered by embedded AgNPs. After introducing the AgNPs into the CPhC structures, the visual appearance of CPhC color films changed markedly (Figure 4a). In addition, Figure 4b shows the back surface photographs of PS CPhC color films with and without AgNPs. In sample B, the visual appearance of the CPhC changes quite remarkably from milky white to intense deep green by introducing AgNPs into the lattice structure, as shown in Figure 4b. This phenomenon shows that AgNPs have similar properties to CB as reported in the literature [13–16]. In consequence, AgNPs may also absorb scattering light and increase the color saturation, thereby producing brighter structural colors of CPhCs. In addition, we also observed the coffee ring of CPhC color films, as shown in Figure 4a. The “coffee ring” effect is a common phenomenon in colloidal fluids [35–37] produced in the process of droplet evaporation, as shown in Figure 2.

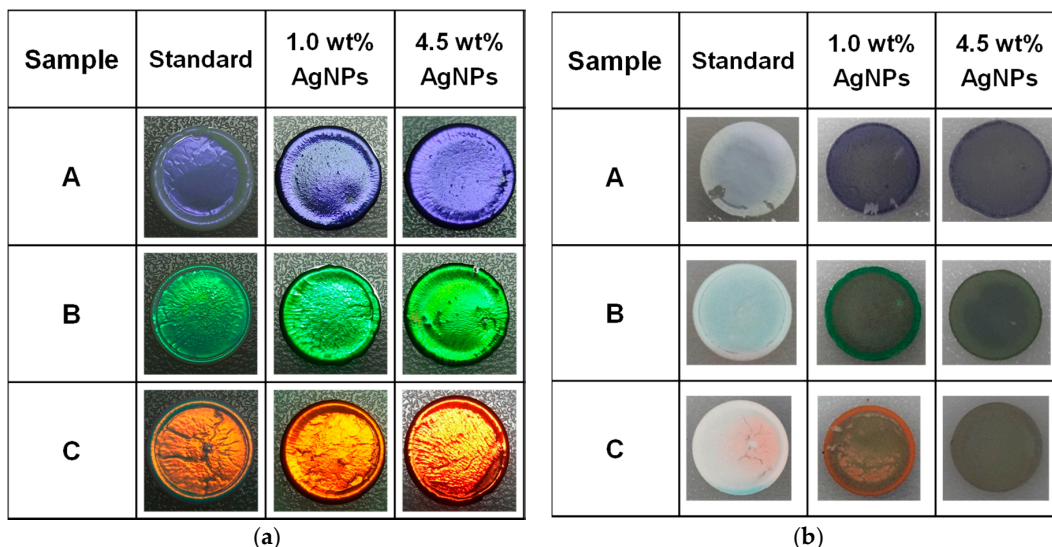


**Figure 4.** (a) Top surface and (b) back surface of AgNPs/PS hybrid CPhC color films (1) without AgNPs (standard) and (2) with 1.0 wt % and (3) 4.5 wt % AgNPs.

### 3. Discussion

The PSBs of all samples were measured using a UV-visible spectrometer with a Xe lamp. Collimated broadband white light from a UV-enhanced Xe lamp was incident on the sample at the surface normal, in which the Ag mirror (*i.e.*, reference for the reflectance measurement) was the incident light of the Xe light source. The light spot size on the sample was approximately 4.0 mm. Fiber optic Y-cables were used for reflectance measurement. Figure 5a–c shows the reflectance spectra of PS CPhC color films with and without AgNPs, in which the  $D_{PS}$  were 170 (sample A), 215 (sample B), and 250 nm (sample C), respectively. PS CPhC color films without AgNPs showed reflectance peaks at 417 (sample A), 515 (sample B), and 601 nm (sample C), which corresponded to blue, green, and red, respectively. After doping 4.5 wt % of AgNPs to the three kinds of PS nanospheres, the CPhC color films displayed the low reflection intensity and red-shift reflectance peaks at 421, 519 and 608 nm, respectively. The reflectance spectra of PS CPhCs with various amounts of AgNPs showed different reflection peak positions, which were in accordance with Bragg's law.

The theoretical reflection wavelengths of Bragg diffraction of AgNPs/PS hybrid CPhC color films were determined using the combined form of Bragg's law and Snell's law. For example, according to the Bragg–Snell law (Equation (1)), the relationship between the reflection peak wavelength  $\lambda_R$  and incident angle  $\alpha$  of an ordered structure is

$$\lambda_R = 2\sqrt{2/3}D_{PS}\sqrt{n_{eff}^2 - \sin^2 \alpha} \quad (1)$$

where  $D_{PS} = 215$  nm is the diameter of PS nanospheres (sample B with 4.5 wt % AgNPs), and  $\lambda_R = 519$  nm at normal incident ( $\alpha = 0^\circ$ ). We obtained  $n_{eff} = 1.483$ , which was the effective refractive index of the medium. Thus, we obtained  $n_{eff} = 1.478$ , which is the effective refractive index of the medium. In this case,  $n_{Ag\_air}$ , which is the refractive index of AgNPs in voids, was obtained using Equation (2):

$$n_{eff}^2 = n_{PS}^2 f_{PS} + n_{Ag\_air}^2 (1 - f_{PS}) \quad (2)$$

where  $n_{PS} = 1.592$  is the refractive index of PS nanospheres, and  $f_{PS} = 0.74$  is the volume fraction of the PS nanosphere. Therefore,  $n_{Ag\_air} = 1.091$  was obtained by calculation. The reflection position slightly red-shifted compared with the original PS CPhCs when AgNPs had adsorbed on PS nanospheres. This adsorption was monitored based on the higher  $n_{Ag\_air}$  than  $n_{air}$ , as shown in Figure 5b. This

phenomenon shows that AgNPs have similar properties to CuO (copper oxide) NPs, as reported in a previous study [23].

In addition, the PS CPhC films containing AgNPs were exhibited weak reflectance because of the overly high concentration of AgNPs (Figure 5a–c). With the increase in AgNPs content, the structural color became brilliant, because scattering and background light were strongly absorbed by settling on the bottom of AgNPs (Figure 4b). Conversely, excessive AgNPs resulted in decreased peak height and loss of brightness because certain AgNPs may cover the surfaces of PS nanospheres by hydrogen bonding or other molecular forces during self-assembly of PS nanospheres into the ordered structures. Thus, more photons were absorbed in the PSB. The brilliance of CPhC color films was effectively enhanced by adding an appropriate amount of AgNPs. Bright structural colors were achieved because of the well-ordered structure, and film color could be tuned by changing the size of PS nanospheres. The effects of the AgNPs content on the reflectance and color of CPhC films are summarized in Figure 5d.

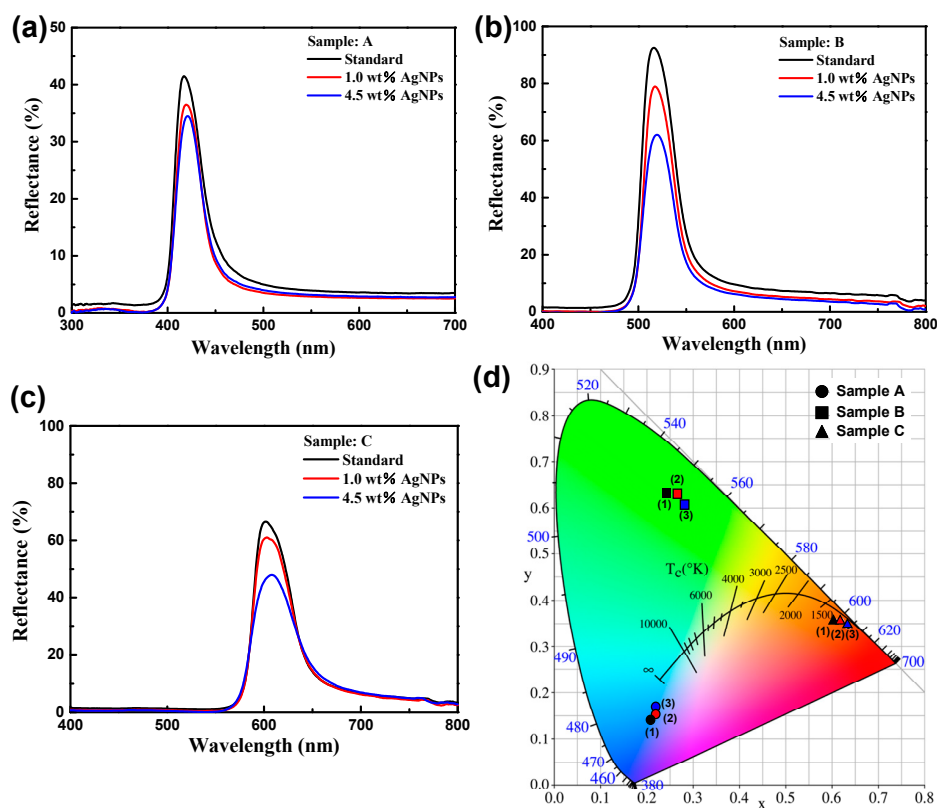


**Figure 5.** Reflection spectra of PS CPhC films with and without AgNPs: (a) sample A (●); (b) sample B (■); and (c) sample C (▲). (d) Commission International d’Eclairage (CIE) chromaticity diagram of AgNPs/PS hybrid CPhC color films for different samples (A–C) and AgNPs contents.

The colors of AgNPs/PS hybrid CPhC color films were determined by the corresponding chromaticity coordinates of the Commission International d’Eclairage (CIE) standard colorimetric system. The visible wavelength (380–700 nm) of the CIE chromaticity diagram visually determined the changes in CPhC structural colors. Color measurement was performed by irradiating the AgNPs/PS hybrid CPhC color films under a D65 light source of the CIE standard illuminant. Subsequently, the reflection spectra obtained from AgNPs/PS hybrid CPhC color films were used to calculate CIE chromaticity coordinates according to SpectraSuite software. The color of CPhC structures was visually presented in the CIE chromaticity diagram, in which the color coordinates indicated the corresponding structural color. For the  $D_{PS}$  of 170 (sample A, ●), 215 (sample B, ■), and 250 nm (sample C, ▲),

the structural colors were blue, green, and red, respectively, as shown in Figure 5d. With the same diameters of PS nanospheres, the incorporation of different AgNPs corresponded to the same color hue but different purities. Not only were the three primary colors for additive or subtractive combination achieved using the AgNPs/PS hybrid CPhC color films, but iridescent derivative colors were also obtained by altering the  $D_{PS}$  (Figure 5). In addition, Figure 5d exhibits slight color shifts for samples A (●), B (■), and C (▲). Nevertheless, AgNPs demonstrated weak tunable structural color capability compared with CuONPs [23]. The AgNPs/PS hybrid CPhC color films exhibited considerable potential to show not only panchromatic colors but also holographic colors. PS nanosphere size and AgNP content could influence the optical properties of CPhC color films.

This study found that AgNPs/PS hybrid CPhC films generally suffer from poor mechanical strength, because of weak interaction among colloidal nanospheres. Several methods have been proposed to enhance the mechanical properties, such as carbon nanotubes (CNTs) [38].

## 4. Materials and Methods

### 4.1. Materials

Styrene (St) was distilled prior before use. Sodium dodecyl sulfate (SDS), potassium persulfate (KPS), sodium bicarbonate ( $\text{NaHCO}_3$ ), and Ag nanopowder (<100 nm particle size; 99.5% trace metal basis) was used as received. Deionized (DI) water (18.2  $\text{M}\Omega \cdot \text{cm}$  resistivity) was purified using the PURELAB purification system.

### 4.2. Synthesis of PS-Based Nanospheres

Monodisperse PS nanospheres were synthesized by the emulsion polymerization method according to a method described previously [23]. The monodisperse PS nanospheres were prepared using St as monomer, SDS as emulsifier, KPS as initiator, and  $\text{NaHCO}_3$  as buffer in the emulsion polymerization process. PS nanosphere powders were purified by dialysis, collected through centrifugation at 15,000 rpm for 1 h, and purified five times through DI water washing before dried in a vacuum-drying oven. By varying the quantity of SDS, colloidal PS nanospheres with different sizes were synthesized using the same method.  $D_{PS}$  was found to be linearly dependent on the amount of SDS.

### 4.3. Attachment of AgNPs to Colloidal PS Latex

Ag nanopowder with 99.5% metal basis was purchased from Sigma–Aldrich. We utilized the random distribution of AgNPs on the PS nanosphere surface. PS latex suspensions containing 500 mg of three different  $D_{PS}$  nanopowder (samples A–C) dispersed in 10 g of DI water at a concentration of approximately 4.8 wt % were prepared by ultrasonication for 8 h. Various 4.8 wt % PS latex suspensions were added with 100 mg (approximately 1.0 wt %) and 500 mg (approximately 4.5 wt %) of Ag nanopowder. AgNP random distribution on the PS surface by electrostatic interactions was allowed to occur with ultrasonication for 8 h, by which unabsorbed AgNPs settled at the bottom of the bottle.

### 4.4. Characterization

The morphologies of the AgNPs/PS hybrid CPhC color films were observed using FESEM (S-4800, Hitachi, Chiyoda, Tokyo), and FETEM (JEM-2100F, JEOL, Tokyo, Japan). EDS (EMAX400, Horiba, Kyoto, Japan) was used to verify the presence of AgNPs on the PS nanosphere surface. The PS nanosphere size distribution was determined using a LPSA (N4 plus; Beckman Coulter, Brea, CA, USA). UV–visible extinction spectra were obtained in standard transmittance mode, and the reflectance and color of AgNPs/PS hybrid CPhC films were measured using a HR2000 spectrometer (Ocean Optics, Winter Park, FL, USA) with unpolarized white light provided by a Xe light source. Fiber optic Y-cables were used for reflection measurement. Color measurement of AgNPs/PS hybrid

CPhCs color films was performed using SpectraSuite software (Ocean Optics) according to the CIE standard colorimetric system. Cover glasses (10 mm in diameter; Marienfeld, München, Germany) were plasma treated (Zepto, Diener, Ebhausen, Germany) to obtain a hydrophilic surface before use. Plasma treatment was conducted in an atmosphere of oxygen with 12.5 SCCM for a step time of 5 min.

## 5. Conclusions

AgNPs/PS hybrid CPhC color films with desirable structural colors were fabricated in this study. AgNPs/PS hybrid CPhC structures could absorb scattering light, thereby remarkably increasing color and producing brilliant tunable structural colors that were visible under natural lighting conditions. The visual appearance of colloidal crystal coatings changed markedly from faint milky white to brilliant colors after doping AgNPs, which absorbed the backward scattering of light. In addition, the measured PSBs of the CPhCs were in accordance with the theoretical calculation. The proposed novel method offers a tunable structural color for future applications in textile fabrics, bionic colors, catalysis, and paints.

**Supplementary Materials:** The following are available online at <http://www.mdpi.com/2073-4352/6/5/61/s1>. Figure S1: FETEM images of (a) AgNP agglomerates at 1.0 wt % concentration and (b) PS CPhC structures with 1.0 wt % AgNPs (sample C). (c) EDS compositional mapping (Ag) scans from the red cross point of image (b). All scale bars are 20 nm. Figure S2: Diameter distribution of PS nanospheres prepared using (a) sample A, (b) sample B, and (c) sample C.

**Acknowledgments:** This work is supported by the Ministry of Science and Technology (MOST) in Taiwan, under contract numbers MOST102-2632-E-035-001-MY3 and MOST103-2221-E-035-029. The authors appreciate the Precision Instrument Support Center of Feng Chia University in providing the fabrication and measurement facilities.

**Author Contributions:** Chun-Feng Lai conceived and designed the experiments; Yu-Chi Wang performed all the experiments; Chun-Feng Lai analyzed the data; Chun-Feng Lai wrote the paper.

**Conflicts of Interest:** The authors declare no conflict of interest.

## Abbreviations

The following abbreviations are used in this manuscript:

PS	polystyrene
CPhCs	colloidal photonic crystals
NPs	nanoparticles
PSB	photonic stop band
CB	carbon black
Au	gold
Ag	silver
LSPR	localized surface plasmon resonance
fcc	face-centered cubic
FESEM	field-emission scanning electron microscopy
FETEM	field-emission transmission electron microscope
DLS	dynamic light scattering
LPSA	laser particle size analyzer
EDS	energy dispersive spectrometer
CIE	Commission International d'Eclairage
wt %	weight percent

## References

1. Cong, H.; Yu, B.; Tang, J.; Li, Z.; Liu, X. Current status and future developments in preparation and application of colloidal crystals. *Chem. Soc. Rev.* **2013**, *42*, 7774–7800. [[CrossRef](#)] [[PubMed](#)]
2. Stein, A.; Wilson, B.E.; Rudisill, S.G. Design and functionality of colloidal-crystal-templated materials-chemical applications of inverse opals. *Chem. Soc. Rev.* **2013**, *42*, 2763–2803. [[CrossRef](#)] [[PubMed](#)]
3. Vogel, N.; Retsch, M.; Fustin, C.A.; Campo, A.D.; Jonas, U. Advances in Colloidal Assembly: The Design of Structure and Hierarchy in Two and Three Dimensions. *Chem. Rev.* **2015**, *115*, 6265–6311. [[CrossRef](#)] [[PubMed](#)]

4. Aguirre, C.I.; Reguera, E.; Stein, A. Tunable Colors in Opals and Inverse Opal Photonic Crystals. *Adv. Funct. Mater.* **2010**, *20*, 2565–2578. [[CrossRef](#)]
5. Li, Y.; Duan, G.; Liu, G.; Cai, W. Physical processes-aided periodic micro/nanostructured arrays by colloidal template technique: Fabrication and applications. *Chem. Soc. Rev.* **2013**, *42*, 3614–3627. [[CrossRef](#)] [[PubMed](#)]
6. Lai, C.F.; Lee, Y.C.; Tsai, T.L. Candlelight LEDs fabricated by using composite silica photonic crystals. *Opt. Mater. Express* **2015**, *5*, 307–313. [[CrossRef](#)]
7. Lai, C.F.; Lee, Y.C.; Kuo, C.T. Saving phosphor by 150% and producing high color-rendering index candlelight LEDs containing composite photonic crystals. *J. Light. Technol.* **2014**, *32*, 1930–1935. [[CrossRef](#)]
8. Klein, S.M.; Manoharan, V.N.; Pine, D.J.; Lange, F.F. Preparation of monodisperse PMMA microspheres in nonpolar solvents by dispersion polymerization with a macromonomeric stabilizer. *Colloid Polym. Sci.* **2003**, *282*, 7–13. [[CrossRef](#)]
9. Zhang, Y.; Dong, B.; Chen, A.; Liu, X.; Shi, L.; Zi, J. Using Cuttlefish Ink as an Additive to Produce Non-iridescent Structural Colors of High Color Visibility. *Adv. Mater.* **2015**, *27*, 4719–4724. [[CrossRef](#)] [[PubMed](#)]
10. Tang, B.; Xu, Y.; Lin, T.; Zhang, S. Polymer opal with brilliant structural color under natural light and white environment. *J. Mater. Res.* **2015**, *30*, 3134–3141. [[CrossRef](#)]
11. Wang, F.; Gou, Z.; Ge, Y.; An, K. Preparation of tunable structural colour film by coating ps with titania on glass. *Micro. Nano Lett.* **2016**, *11*, 50–53. [[CrossRef](#)]
12. Wang, F.; Zhang, X.; Zhang, L.; Cao, M.; Lin, Y.; Zhu, J. Rapid fabrication of angle-independent structurally colored films with a superhydrophobic property. *Dyes Pigment* **2016**, *130*, 202–208. [[CrossRef](#)]
13. Cong, H.; Yu, B.; Wang, S.; Qi, L.; Wang, J.; Ma, Y. Preparation of iridescent colloidal crystal coatings with variable structural colors. *Opt. Express* **2013**, *21*, 17831–17838. [[CrossRef](#)] [[PubMed](#)]
14. Aguirre, C.I.; Reguera, E.; Stein, A. Colloidal Photonic Crystal Pigments with Low Angle Dependence. *ACS Appl. Mater. Interfaces* **2010**, *2*, 3257–3262. [[CrossRef](#)] [[PubMed](#)]
15. Shen, Z.; Shi, L.; You, B.; Wu, L.; Zhao, D. Large-scale fabrication of three-dimensional ordered polymer films with strong structure colors and robust mechanical properties. *J. Mater. Chem.* **2012**, *22*, 8069–8075. [[CrossRef](#)]
16. Wang, W.; Tang, B.; Ma, W.; Zhang, J.; Ju, B.; Zhang, S. Easy approach to assembling a biomimetic color film with tunable structural colors. *J. Opt. Soc. Am. A* **2015**, *32*, 1109–1117. [[CrossRef](#)] [[PubMed](#)]
17. Pursiainen, O.L.; Baumberg, J.J.; Winkler, H.; Viel, B.; Spahn, P.; Ruhl, T. Nanoparticle-tuned structural color from polymer opals. *Opt. Express* **2007**, *15*, 9553–9561. [[CrossRef](#)] [[PubMed](#)]
18. Yamada, Y.; Ishii, M.; Nakamura, T.; Yano, K. Artificial Black Opal Fabricated from Nanoporous Carbon Spheres. *Langmuir* **2010**, *26*, 10044–10049. [[CrossRef](#)] [[PubMed](#)]
19. Wang, F.; Zhang, X.; Lin, Y.; Wang, L.; Zhu, J. Structural Coloration Pigments based on Carbon Modified ZnS@SiO<sub>2</sub> Nanospheres with Low-Angle Dependence, High Color Saturation, and Enhanced Stability. *ACS Appl. Mater. Interfaces* **2016**, *8*, 5009–5016. [[CrossRef](#)] [[PubMed](#)]
20. Wang, F.; Zhang, X.; Lin, Y.; Wang, L.; Qin, Y.; Zhu, J. Fabrication and characterization of structurally colored pigments based on carbon-modified ZnS nanospheres. *J. Mater. Chem. C* **2016**, *4*, 3321–3327. [[CrossRef](#)]
21. Erola, M.O.A.; Philip, A.; Ahmed, T.; Suvanto, S.; Pakkanen, T.T. Fabrication of Au- and Ag-SiO<sub>2</sub> inverse opals having both localized surface plasmon resonance and Bragg diffraction. *J. Sol. Stat. Chem.* **2015**, *230*, 209–217. [[CrossRef](#)]
22. Yu, B.; Zhai, F.; Cong, H.; Yang, D. Photosensitive polystyrene/silver bromide hybrid colloidal crystals as recoverable colorimetric naked eye probes for bromine gas sensing. *J. Mater. Chem. C* **2016**, *4*, 1386–1391. [[CrossRef](#)]
23. Lai, C.F.; Wang, Y.C.; Wu, C.L.; Zeng, J.Y.; Lin, C.F. Preparation of a colloidal photonic crystal containing CuO nanoparticles with tunable structural colors. *RSC Adv.* **2015**, *5*, 105200–105205. [[CrossRef](#)]
24. Mu, Z.; Zhao, X.; Huang, Y.; Lu, M.; Gu, Z. Photonic Crystal Hydrogel Enhanced Plasmonic Staining for Multiplexed Protein Analysis. *Small* **2015**, *11*, 6036–6043. [[CrossRef](#)] [[PubMed](#)]
25. Zhao, X.; Xue, J.; Mu, Z.; Huang, Y.; Lu, M.; Gu, Z. Gold nanoparticle incorporated inverse opal photonic crystal capillaries for optofluidic surface enhanced Raman spectroscopy. *Biosens. Bioelectron.* **2015**, *72*, 268–274. [[CrossRef](#)] [[PubMed](#)]
26. Ji, X.; Song, X.; Li, J.; Bai, Y.; Yang, W.; Peng, X. Size Control of Gold Nanocrystals in Citrate Reduction: The Third Role of Citrate. *J. Am. Chem. Soc.* **2007**, *129*, 13939–13948. [[CrossRef](#)] [[PubMed](#)]

27. Yadav, A.; Danesh, M.; Zhong, L.; Cheng, G.J.; Jiang, L.; Chi, L. Spectral plasmonic effect in the nano-cavity of dye-doped nanosphere-based photonic crystals. *Nanotechnology* **2016**, *27*, 165703. [[CrossRef](#)] [[PubMed](#)]
28. Wang, D.; Zhou, F.; Wang, C.; Liu, W. Synthesis and characterization of silver nanoparticle loaded mesoporous TiO<sub>2</sub> nanobelts. *Microporous Mesop. Mater.* **2008**, *116*, 658–664. [[CrossRef](#)]
29. Sondi, I.; Salopekk-Sondi, B. Silver nanoparticles as antimicrobial agent: A case study on *E. coli* as a model for Gram-negative bacteria. *J. Colloid Interfaces Sci.* **2004**, *275*, 177–182. [[CrossRef](#)] [[PubMed](#)]
30. Ashokkumar, S.; Ravi, S.; Kathiravan, V.; Velmurugan, S. Synthesis, characterization and catalytic activity of silver nanoparticles using *Tribulus terrestris* leaf extract. *Spectrochim. Act. Part A Mol. Biomol. Spectrosc.* **2014**, *121*, 88–93. [[CrossRef](#)] [[PubMed](#)]
31. Haider, A.; Kang, I.K. Preparation of Silver Nanoparticles and Their Industrial and Biomedical Applications: A Comprehensive Review. *Adv. Mater. Sci. Eng.* **2015**, *2015*, 165257. [[CrossRef](#)]
32. Gabriel Ortega-Mendoza, J.; Padilla-Vivanco, A.; Tozqui-Quitl, C.; Zaca-Moran, P.; Villegas-Hernandez, D.; Chavez, F. Optical Fiber Sensor Based on Localized Surface Plasmon Resonance Using Silver Nanoparticles Photodeposited on the Optical Fiber End. *Sensors* **2014**, *14*, 18701–18710. [[CrossRef](#)] [[PubMed](#)]
33. Henglein, A. Colloidal Silver Nanoparticles: Photochemical Preparation and Interaction with O<sub>2</sub>, CCl<sub>4</sub>, and Some Metal Ions. *Chem. Mater.* **1998**, *10*, 444–450. [[CrossRef](#)]
34. Pal, S.; Tak, Y.K.; Song, J.M. Does the Antibacterial Activity of Silver Nanoparticles Depend on the Shape of the Nanoparticle? A Study of the Gram-Negative Bacterium *Escherichia Coli*. *Appl. Environ. Microbiol.* **2007**, *73*, 1712–1720. [[CrossRef](#)] [[PubMed](#)]
35. Deegan, R.D.; Bakajin, O.; Dupont, T.F.; Huber, G.; Nagel, S.R.; Witten, T.A. Capillary flow as the cause of ring stains from dried liquid drops. *Nature* **1997**, *389*, 827–829. [[CrossRef](#)]
36. Deegan, R.D.; Bakajin, O.; Dupont, T.F.; Huber, G.; Nagel, S.R.; Witten, T.A. Contact line deposits in an evaporating drop. *Phys. Rev. E* **2000**, *62*, 756. [[CrossRef](#)]
37. Deegan, R.D. Pattern formation in drying drops. *Phys. Rev. E* **2000**, *61*, 475. [[CrossRef](#)]
38. Li, F.; Tang, B.; Xiu, J.; Zhang, S. Hydrophilic Modification of Multi-Walled Carbon Nanotube for Building Photonic Crystals with Enhanced Color Visibility and Mechanical Strength. *Molecules* **2016**, *21*, 547. [[CrossRef](#)] [[PubMed](#)]



© 2016 by the authors; licensee MDPI, Basel, Switzerland. This article is an open access article distributed under the terms and conditions of the Creative Commons Attribution (CC-BY) license (<http://creativecommons.org/licenses/by/4.0/>).